An efficient hybrid pseudospectral/finite-difference scheme for solving TTI pure P-wave equation

Ge Zhan, King Abdullah University of Science and Technology (KAUST), Reynam C. Pestana, CPGG/UFBA and INCT-GP/CNPQ and Paul L. Stoffa, IG, University of Texas at Austin

This paper was prepared for presentation at the 13th International Congress of the Brazilian Geophysical Society, held in Rio de Janeiro, Brazil, August 26-29, 2013.

Abstract

The pure P-wave equation for modeling and migration in tilted transversely isotropic (TTI) media has attracted more and more attention in imaging seismic data with anisotropy. The desirable feature is that it is absolutely free of shear-wave artifacts and the consequent alleviation of numerical instabilities generally suffered by some systems of coupled equations. However, due to several forward-backward Fourier transforms in wavefield updating at each time step, the computational cost is significant, and thereby hampers its prevalence. We propose to use a hybrid pseudospectral (PS) and finite-difference (FD) scheme to solve the pure P-wave equation. In the hybrid solution, most of the cost-consuming wavenumber terms in the equation are replaced by inexpensive finite-difference operators, which in turn accelerates the computation and reduces the computational cost. To demonstrate the benefit in cost saving of the new scheme, 2D and 3D reverse-time migration (RTM) examples using the hybrid solution to the pure P-wave equation are carried out, and respective runtimes are listed and compared. Numerical results show that the hybrid strategy demands less computation time and is faster than using the pseudospectral method alone. Furthermore, this new TTI RTM algorithm with the hybrid method is less computationally expensive than that with the finite-difference solution to conventional TTI coupled equations.

Introduction

Various methods for modeling anisotropic acoustic seismic waves (Alkhalifah, 1998; Zhou et al., 2006a; Du et al., 2008) as well as wavefronts and rays (Bos and Slawinski, 2010; Epstein et al., 2012) have been proposed and developed, especially for vertical transversely isotropic (VTI) and tilted transversely isotropic (TTI) media. In general, we can divide those methods into two broad categories: methods that suffered from shear-wave artifacts, usually known as coupled equations where P and shear-wave are coupled together (Alkhalifah, 2000; Zhou et al., 2006a,b; Fletcher et al., 2009; Fowler et al., 2010; Duveneck and Bakker, 2011); and pure P-wave (or decoupled) equations which are free of shear-wave artifacts (Etgen and Brandsberg-Dahl, 2009; Liu et al., 2009; Chu et al., 2011; Pestana et al., 2012; Zhan et al., 2012).

The pure P-wave equation in the system of decoupled equations of Zhan et al. (2012) is in the wavenumber domain, and at each time step it requires eight fast Fourier transforms (FFTs) for 2D, and twenty-two FFTs for 3D. This imposes an unrealistic demand for practical migration of large-scale 3D field seismic data sets. In the work presented below, we follow the same derivations of Pestana et al. (2012) and Zhan et al. (2012), but reorganize and rewrite the wavenumber domain equation in a compact way for efficient computation. After some algebraic manipulations, it still requires eight FFTs per time step for 2D computation with the new formulation, but the number of FFTs needed per time step for 3D is reduced from twenty-two to fourteen.

To further reduce the computational cost introduced by numerous FFTs, we propose a hybrid pseudospectral and finite-difference scheme to evaluate the equation by using the relation between the spatial derivative and the operator in the wavenumber domain. Both 2D and 3D reverse-time migration (RTM) examples with the new hybrid algorithm are tested and demonstrated to validate the uplift in computational efficiency.

Equations

Isotropic wave equation

The constant-density acoustic wave equation in isotropic media is

$$\frac{\partial^2 u(\vec{x},t)}{\partial t^2} = L^2 u(\vec{x},t), \tag{1}$$

where $u(\vec{x},t)$ is the pressure wavefield at spatial location $\vec{x} = (x,y,z)$ and time t; $L^2 = v^2(\vec{x})\nabla^2$, where $v(\vec{x})$ is the P-wave velocity in the medium, and ∇^2 is the Laplacian defined as $\nabla^2 = \partial_x^2 + \partial_y^2 + \partial_z^2$. An efficient numerical solution of the wave equation on a discrete grid is our main interest. To solve the discretized version of equation 1, we approximate the temporal (left) and spatial (right) derivatives in the equation, where the time derivative is approximated by a second-order finite-difference approximation

$$u(\vec{x},t+\Delta t) = 2u(\vec{x},t) - u(\vec{x},t-\Delta t) - \Delta t^2 \left[-L^2 u(\vec{x},t) \right]. \tag{2}$$

Here Δt denotes the length of a discrete time step.

The pseudospectral method (Reshef et al., 1988) is known as a highly accurate scheme for approximating the Laplacian operator. In doing so, the numerical errors in the solution of the wave equation are only dominated by the temporal discretization. For the isotropic case, the $-L^2$ operator in equation 2 can be expressed in the wavenumber domain

$$-L^2 = v_v^2\left(k_x^2 + k_y^2 + k_z^2\right) = v_v^2(k_r^2 + k_z^2) = v_v^2 k_\rho^2, \qquad (3)$$

where v_v is the velocity of a wave traveling vertically along the axis of symmetry; k_x, k_y and k_z are the spatial wavenumbers in the x, y and z directions, respectively; $k_r^2 = k_x^2 + k_y^2$, and $k_\rho^2 = k_x^2 + k_y^2 + k_z^2$.

VTI pure P-wave equation

In the case of VTI, based on Harlan (1995) and later rediscovered by Etgen and Brandsberg-Dahl (2009), Crawley et al. (2010), Pestana et al. (2012) and Zhan et al. (2012) where they started from the exact phase velocity expression for VTI media, equation 3 becomes

$$-L^2 = v_v^2 k_z^2 + v_h^2 k_r^2 + \left(v_n^2 - v_h^2\right)\frac{k_r^2 k_z^2}{k_\rho^2}. \qquad (4)$$

Here, $v_n = v_v\sqrt{1+2\delta}$ and $v_h = v_v\sqrt{1+2\varepsilon}$ represent the normal moveout (NMO) velocity and the P-wave velocity in the horizontal direction, respectively; δ and ε are the Thomsen (1986) anisotropy parameters.

The resulting anisotropic wave equation derived in this way is known as the pure P-wave or decoupled equation, where the P-wave and shear-wave components are completely separated and there are no spurious shear-wave artifacts in the P-wave simulation.

TTI pure P-wave equation

A similar expression for TTI media can be deduced from equation 4 through variable exchanges (Zhan et al., 2012)

$$-L^2 = v_v^2 k_{\tilde{z}}^2 + v_h^2 k_{\tilde{r}}^2 + \left(v_n^2 - v_h^2\right)\frac{k_{\tilde{r}}^2 k_{\tilde{z}}^2}{k_\rho^2}, \qquad (5)$$

where $k_{\tilde{r}}^2 = k_{\tilde{x}}^2 + k_{\tilde{y}}^2$ with $k_{\tilde{x}}$, $k_{\tilde{y}}$ and $k_{\tilde{z}}$ representing the spatial wavenumbers in the rotated coordinate system

$$\begin{bmatrix} k_{\tilde{x}} \\ k_{\tilde{y}} \\ k_{\tilde{z}} \end{bmatrix} = \begin{bmatrix} \cos\theta\cos\phi & \cos\theta\sin\phi & \sin\theta \\ -\sin\phi & \cos\phi & 0 \\ -\sin\theta\cos\phi & -\sin\theta\sin\phi & \cos\theta \end{bmatrix} \begin{bmatrix} k_x \\ k_y \\ k_z \end{bmatrix}. \qquad (6)$$

Here θ and ϕ are dip and azimuth, and the following relation holds

$$k_{\tilde{x}}^2 + k_{\tilde{y}}^2 + k_{\tilde{z}}^2 = k_x^2 + k_y^2 + k_z^2. \qquad (7)$$

In the case of elliptical anisotropy where $\varepsilon = \delta$ (i.e., $v_h = v_n$), the last term of equation 5 with wavenumbers in the denominator disappears. Therefore, the first two terms in equation 5 represent the properties of elliptical anisotropy, while the last term compensates for anelliptical anisotropic effects due to the rotation of the symmetry axis.

According to the rotation matrix 6, and denoting $\Gamma_x = \sin\theta\cos\phi$, $\Gamma_y = \sin\theta\sin\phi$ and $\Gamma_z = -\cos\theta$, we can rewrite $k_{\tilde{z}}$ in the rotated system in terms of k_x, k_y and k_z

$$\begin{aligned} k_{\tilde{z}} &= -\left(k_x\sin\theta\cos\phi + k_y\sin\theta\sin\phi - k_z\cos\theta\right) \\ &= -\left(k_x\Gamma_x + k_y\Gamma_y + k_z\Gamma_z\right). \qquad (8) \end{aligned}$$

Hence the three wavenumber terms in equation 5 can be computed in the following order

$$\begin{aligned} k_{\tilde{z}}^2 &= k_x^2\Gamma_{xx} + k_y^2\Gamma_{yy} + k_z^2\Gamma_{zz} \\ &\quad + 2\left(k_x k_y\Gamma_{xy} + k_y k_z\Gamma_{yz} + k_x k_z\Gamma_{xz}\right) = V, \qquad (9a) \end{aligned}$$

$$k_{\tilde{r}}^2 = k_\rho^2 - V = H, \qquad (9b)$$

$$\begin{aligned} \frac{k_{\tilde{r}}^2 k_{\tilde{z}}^2}{k_\rho^2} &= \left[\frac{k_x^2}{k_\rho^2}\Gamma_{xx} + \frac{k_y^2}{k_\rho^2}\Gamma_{yy} + \frac{k_z^2}{k_\rho^2}\Gamma_{zz}\right. \\ &\quad \left. + 2\left(\frac{k_x k_y}{k_\rho^2}\Gamma_{xy} + \frac{k_y k_z}{k_\rho^2}\Gamma_{yz} + \frac{k_x k_z}{k_\rho^2}\Gamma_{xz}\right)\right] H = T, \qquad (9c) \end{aligned}$$

where $\Gamma_{ij} = \Gamma_i\Gamma_j$; V, H and T are differential operators in the wavenumber domain that operate along the symmetry axis direction, the symmetry plane perpendicular to the symmetry axis, and the tilted direction, respectively.

Numerical Implementations

Pseudospectral scheme

The pseudospectral method is proposed by Kosloff and Baysal (1982), which uses Fourier transformation, multiplication by ik in the wavenumber domain, and inverse Fourier transformation back to the spatial domain to compute the spatial derivatives. Differential operators V, H and T in equation 9 are written in the wavenumber domain and are easily evaluated there with the pseudospectral method. Meanwhile, as in the pseudospectral method, performing the operations in the wavenumber domain guarantees that it will not suffer from numerical dispersion.

Substituting equations 5 and 9 into equation 2, we write the TTI pure P-wave equation as

$$\begin{aligned} u(\vec{x}, t+\Delta t) &= 2u(\vec{x},t) - u(\vec{x}, t-\Delta t) \\ &- \Delta t^2\left\{\left[v_v^2 V + v_h^2 H + (v_n^2 - v_h^2)T\right]u(\vec{x},t)\right\} \\ &= u(\vec{x},t) - u(\vec{x}, t-\Delta t) \\ &- \Delta t^2\left\{v_v^2\mathscr{F}^{-1}\left[V\mathscr{F}[u(\vec{x},t)]\right] + v_h^2\mathscr{F}^{-1}\left[H\mathscr{F}[u(\vec{x},t)]\right]\right. \\ &+ \left.(v_n^2 - v_h^2)\mathscr{F}^{-1}\left[T\mathscr{F}[u(\vec{x},t)]\right]\right\}, \qquad (10) \end{aligned}$$

where $\mathscr{F}$ and $\mathscr{F}^{-1}$ are forward and inverse FFTs, respectively.

From the above equations, we can see that at each time step of a 3D simulation, the evaluation of the differential operator V demands at least a 3D forward FFT of the wavefield plus six 3D inverse FFTs. A similar analysis applies to the differential operator T as well. Therefore, a total of fourteen 3D FFTs are required to simulate the pure P-wave wavefield at each time step in a TTI medium. When it comes to 2D, all k_y terms are eliminated, and thus only eight 2D FFTs are needed.

Hybrid pseudospectral/finite-difference scheme

During each time step, the TTI pure P-wave computation in equation 10 requires two forward FFTs and twelve inverse FFTs, which is computationally intensive. By revisiting equation 9, we find that due to the appearance of the wavenumbers in the denominators, equation 9c must be evaluated using the pseudospectral method and it would be difficult to derive pure finite-difference operators that correspond to the six right-hand-side terms. However, there are no such terms in equations 9a and 9b. To greatly reduce the computation cost while avoiding spurious shear-wave artifacts as well as numerical instabilities, we propose a hybrid pseudospectral/finite-difference scheme to evaluate the TTI pure P-wave equation given in equation 10. That is, transforming equations 9a and 9b using the relations $k_x \leftrightarrow -i\frac{\partial}{\partial x}$, $k_y \leftrightarrow -i\frac{\partial}{\partial y}$, $k_z \leftrightarrow -i\frac{\partial}{\partial z}$ yields

$$\begin{aligned} k_{\tilde{z}}^2 \leftrightarrow & -\left[\frac{\partial^2}{\partial x^2}\Gamma_{xx} + \frac{\partial^2}{\partial y^2}\Gamma_{yy} + \frac{\partial^2}{\partial z^2}\Gamma_{zz}\right. \\ & \left. + 2\left(\frac{\partial^2}{\partial x \partial y}\Gamma_{xy} + \frac{\partial^2}{\partial y \partial z}\Gamma_{yz} + \frac{\partial^2}{\partial x \partial z}\Gamma_{xz}\right)\right] = V', \end{aligned} \tag{11a}$$

$$k_{\tilde{r}}^2 \leftrightarrow -\left(\frac{\partial^2}{\partial x^2} + \frac{\partial^2}{\partial y^2} + \frac{\partial^2}{\partial z^2}\right) - V' = H', \tag{11b}$$

where V' and H' can be approximated by finite-difference operators applied along the symmetry axis and symmetry plane, respectively. Spatial derivatives in the above equation can be cheaply computed using a second, fourth or higher order finite-difference scheme instead of using FFTs back and forth.

Although the wavenumber terms in equation 9c can not all be replaced by corresponding finite-difference operators, they could be partially approximated as follows

$$\begin{aligned} \frac{k_{\tilde{r}}^2 k_{\tilde{z}}^2}{k_\rho^2} &= \left[k_x \frac{k_x}{k_\rho^2}\Gamma_{xx} + k_y \frac{k_y}{k_\rho^2}\Gamma_{yy} + k_z \frac{k_z}{k_\rho^2}\Gamma_{zz}\right. \\ & \left. + 2\left(k_y \frac{k_x}{k_\rho^2}\Gamma_{xy} + k_z \frac{k_y}{k_\rho^2}\Gamma_{yz} + k_x \frac{k_z}{k_\rho^2}\Gamma_{xz}\right)\right] H \\ &= \left[(k_x\Gamma_{xx} + 2k_y\Gamma_{xy})\frac{k_x}{k_\rho^2} + (k_y\Gamma_{yy} + 2k_z\Gamma_{yz})\frac{k_y}{k_\rho^2}\right. \\ & \left. + (k_z\Gamma_{zz} + 2k_x\Gamma_{xz})\frac{k_z}{k_\rho^2}\right] H \\ &\leftrightarrow \left[\left(\frac{\partial}{\partial x}\Gamma_{xx} + 2\frac{\partial}{\partial y}\Gamma_{xy}\right)\frac{-ik_x}{k_\rho^2}\right. \\ & \left. + \left(\frac{\partial}{\partial y}\Gamma_{yy} + 2\frac{\partial}{\partial z}\Gamma_{yz}\right)\frac{-ik_y}{k_\rho^2} + \left(\frac{\partial}{\partial z}\Gamma_{zz} + 2\frac{\partial}{\partial x}\Gamma_{xz}\right)\frac{-ik_z}{k_\rho^2}\right] H \\ &= T'. \end{aligned} \tag{11c}$$

Notice that the number of wavenumber terms in equation 11c is reduced from six to three. And T' can now be approximated by finite-difference operators as well as V' and H'.

Therefore, the resulting hybrid solution to the TTI pure P-wave equation becomes

$$\begin{aligned} u(\vec{x}, t+\Delta t) &= 2u(\vec{x}, t) - u(\vec{x}, t-\Delta t) \\ - \quad & \Delta t^2 \left[v_v^2 V' + v_h^2 H' + (v_n^2 - v_h^2) T'\right] u(\vec{x}, t). \end{aligned} \tag{12}$$

Noticeably, the proposed hybrid strategy only requires four (one forward and three inverse) 3D FFTs per time step in simulating a pure P-wave propagation in a 3D TTI medium. For a 2D model, the number of FFTs reduces to three per time step with the hybrid method.

Comparison of two schemes

The most computationally intensive parts in solving the TTI pure P-wave equation are the FFT calculations, therefore we need to count and compare the total number of FFTs in each scheme. Table 1 displays the number of FFTs in modeling the TTI wavefield at a time step with the pure P-wave equation by the standard pseudospectral scheme and the new hybrid scheme. Obviously, the number of FFTs using the hybrid method is reduced by more than half in comparison with that using the pseudospectral method, which indicates that the hybrid algorithm is more computationally efficient compared to the standard pseudospectral scheme. Nevertheless, the disadvantage of the hybrid scheme is that it is no longer as accurate as the standard pseudospectral scheme.

Table 1: Number of FFTs per time step in simulating the TTI wavefield: pseudospectral scheme versus hybrid scheme.

dimension / method	**2D**	**3D**
PS	8	14
Hybrid	3	4

Accuracy comparison

For the proposed hybrid pseudospectral/finite-difference method, the costs of derivative calculations are reduced at the expense of the precision, as well as the accuracy of the solution, because some of the wavenumber operators are substituted by finite-difference approximations. To demonstrate the consequent accuracy loss, we conduct a 2D modeling test on a simple 5-layer TTI model. Figure 1 displays the model parameters that used in this test. The spacial interval of the computational grid is $10\ m$, and the maximum frequency of the source wavelet is $30\ Hz$.

First, equation 10 using the standard pseudospectral method is implemented. Then equation 12 using the hybrid method is computed, where the spatial derivatives in equations 11a, 11b, and 11c are approximated and calculated using second, fourth and eighth-order centered finite-difference schemes from Taylor series expansions, respectively. To check the amplitude differences, three wiggle traces at zero/middle/far offsets computed using different methods are plotted and compared in Figure 2. As we can see from Figure 2, amplitudes computed from the pseudospectral method and the hybrid method with the eighth-order finite-difference scheme are perfectly matched. And the computational costs of these two methods are almost equivalent. When the fourth-order finite-difference scheme is used, all major amplitudes from shallow to deep are still well matched to the pseudospectral result, except that some tiny discrepancies start to appear due to numerical dispersion. However, the runtime is reduced by half. A more compact second-order finite-difference scheme may further improve the computational efficiency, however, both the amplitude discrepancies and phase errors are maximized due to the strong dispersive behavior associated with smaller stencils.

According to the above analysis, in latter numerical examples, the fourth-order finite-difference scheme is chosen to compute spatial derivatives in the hybrid method in terms of accuracy and efficiency.

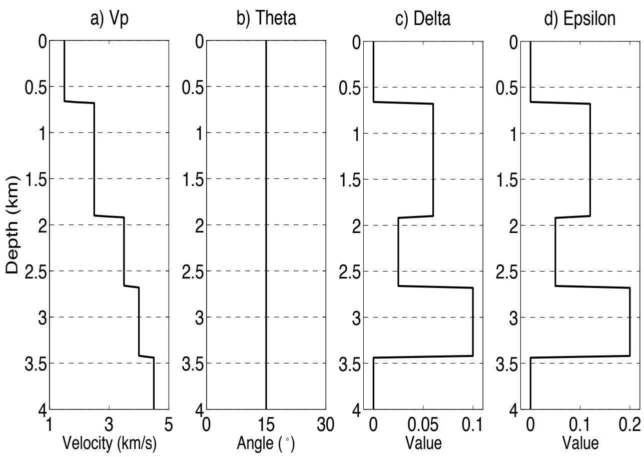

Figure 1: Anisotropic model parameters used in the accuracy test.

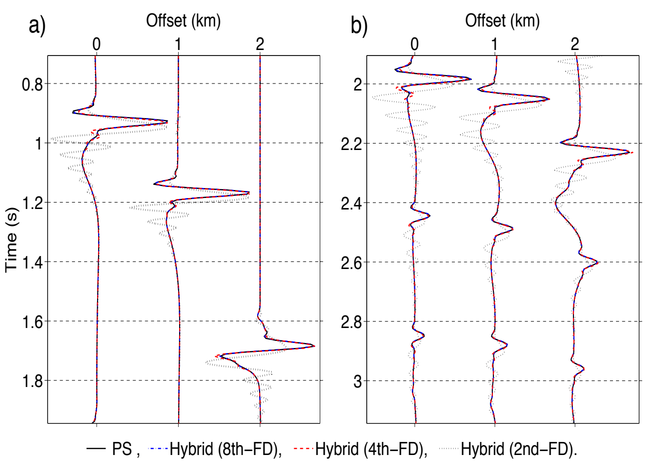

Figure 2: Three traces computed from the 2D 5-layer TTI model are displayed in wiggle mode. (a) compares the first (strongest) reflection event, while (b) compares lower (weak) reflections.

Computation Examples

Computation examples associated with the BP 2D TTI model as well as a 3D salt dome model are now presented to validate the proposed hybrid pseudospectral/finite-difference scheme. TTI RTM algorithms with the pure P-wave equation using both the pseudospectral method and the hybrid method are implemented. Computational costs of running single common-shot-gather (CSG) migration with different approaches are demonstrated. For comparison, standard isotropic RTM, conventional VTI coupled equations (equations 5a and 5b of Du et al. (2008)) and TTI coupled equations (equations 2 and 3 of Fletcher et al. (2009)) using the finite-difference scheme are also implemented and compared.

2D example

The grid size of the computational 2D domain is 1001 grid points in Z and 1061 grid points in X, and a total number of 12267 time steps is computed for both forward propagation and back propagation in migrating a CSG. The computational costs for different RTM strategies running on a 12-core Intel Xeon computing node are listed in Table 2, and the corresponding histogram is displayed in Figure 3.

Table 2: 2D 1-shot RTM runtime comparison using different schemes.

method / media	**2D Runtime ($mins$)**		
	FD	PS	Hybrid
Isotropic	1.9	16.4	–
VTI	9.2	28.0	–
TTI	68.7	94.4	65.5

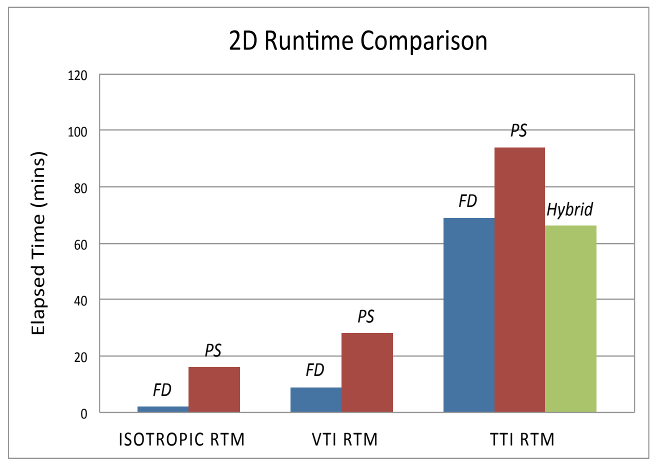

Figure 3: Histogram comparison of the 2D RTM runtimes.

From the runtime comparison, we see that a transfer from isotropy to anisotropy complicates the RTM algorithm by taking into account two or more anisotropic parameters, which results in gradually increasing computational costs with increasing anisotropic complexities. We also notice that the standard pseudospectral method costs much more than the conventional finite-difference approach due to the introduced FFTs for better accuracy. However, by solving the TTI pure P-wave equation in a hybrid method, the RTM cost per shot (24534 time steps in total) is reduced from 94.4 $mins$ to 65.5 $mins$ with the pseudospectral method, where a saving of 31% in computational cost is achieved. And it is even less expensive than the finite-difference solution for the TTI coupled equations (68.7 $mins$ per shot), which usually suffers from shear-wave artifacts.

A stacked TTI RTM image of all 1641 CSGs using the hybrid solution to the pure P-wave equation is shown in Figure 4(b)a. It is almost a perfect replication of the actual reflectivity model as shown in Figure 4(b)b except for some white shadows due to imperfect illuminations.

3D example

The 2D example shown above demonstrated the efficiency of the hybrid strategy. To further examine the performance

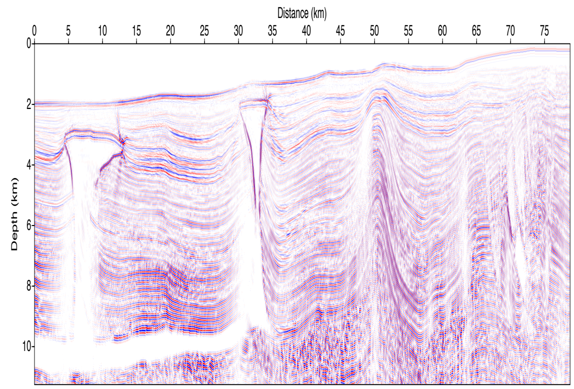

(a)

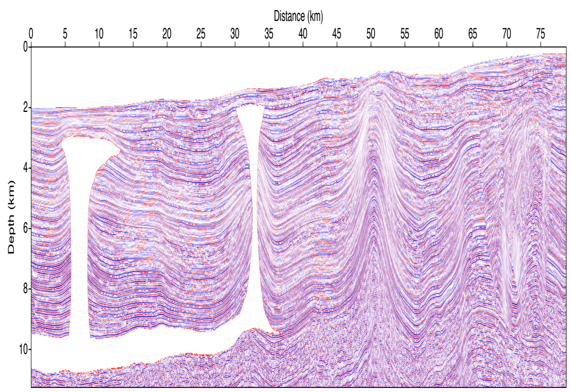

(b)

Figure 4: TTI RTM image of the BP 2D TTI model in (a) is compared with the actual reflectivity model in (b).

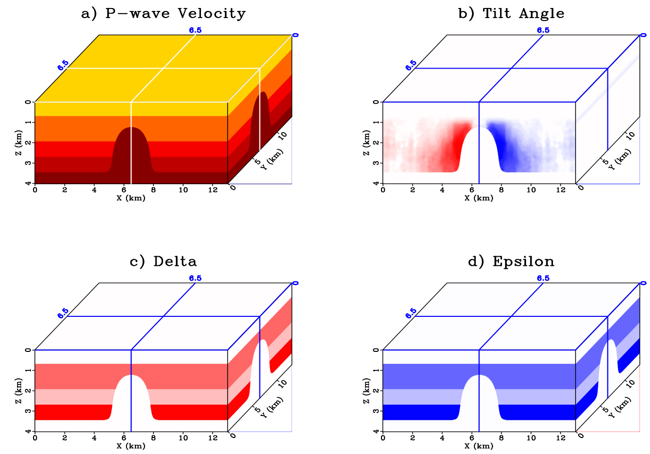

Figure 5: 3D salt dome models: a) v_v and b) θ, c) and d) are Thomsen's parameters δ and ε. The front frame and side frame correspond to 2D slices at Y=6.5 km and X=6.5 km, respectively.

Table 3: 3D 1-shot RTM runtime comparison using different schemes.

method / media	**3D Runtime** ($mins$)		
	FD	PS	Hybrid
Isotropic	23.7	35.4	–
VTI	39.2	50.1	–
TTI	98.2	138.5	94.3

of the hybrid scheme, we test it on a 3D TTI salt dome model.

The models shown in Figure 5 contain five major layers: a water layer, three sedimentary layers with a salt dome embedded in the middle center, and the salt base. The water layer (v_v=1.5 km/s) and the salt (v_v=4.5 km/s) are set to be isotropic (δ=ε=0, θ=0°). And the three sedimentary layers are TTI media with $v_v = 2.5\ km/s, 3.5\ km/s, 4.0\ km/s$ (Figure 5a); $\delta = 0.06, 0.025, 0.1$ (Figure 5c) and $\varepsilon = 0.12, 0.05, 0.2$ (Figure 5d) from shallow to deep. A simple 2.5D tilt angle model (ranges from $-50°$ to $50°$) was adopted with a tilt axis normal to the salt flank (Figure 5b). A constant $\phi = 15°$ is used in this case.

The 3D model has 201 grid points along Z, and 651 grid points along X and Y with a uniform grid point spacing of $20\ m$ in all three directions. For each CSG, the 3D RTM used a local computation grid of 301x401x401 (100 grid points padding in each direction) with a total of 4802 time steps in both the forward and backward propagation operations. Table 3 lists the runtimes of the 3D TTI RTM using one CSG on the 12-core computing node. The isotropic and VTI RTM runtime results are also presented for comparison. These computational costs with different RTM algorithms are then graphically illustrated in Figure 6.

For the 3D model, the hybrid method is still faster than the pseudospectral method by around 29%, this is because more than half the number of 3D FFTs are replaced by less expensive finite-difference calculations. Besides, just like we saw in the 2D case, the hybrid scheme in 3D achieves an even better computational efficiency in comparison with the standard finite-difference solution to the TTI coupled equations. Figure 7 displays the TTI RTM image of this 3D salt dome model.

CONCLUSIONS

We have rewritten the TTI pure P-wave equation in a form which reduces the number of FFTs per time step simulation. Also, a hybrid pseudospectral/finite-difference is proposed to solve this equation, where wavenumber operators are replaced by inexpensive finite-difference spatial operators. The computational costs of TTI RTM with the hybrid method are reduced by 31% for the 2D case and 29% for the 3D case. Therefore, the hybrid pseudospectral/finite-difference scheme makes the TTI pure P-wave equation more practical and realistic for industrial-scale 3D migration problems.

ACKNOWLEDGMENTS

We thank the Supercomputing Laboratory at King Abdullah University of Science and Technology (KAUST) in Thuwal,

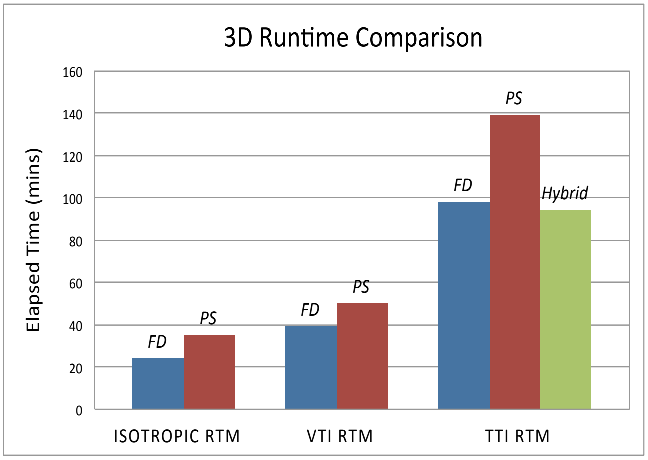

Figure 6: Histogram comparison of the 3D RTM runtimes.

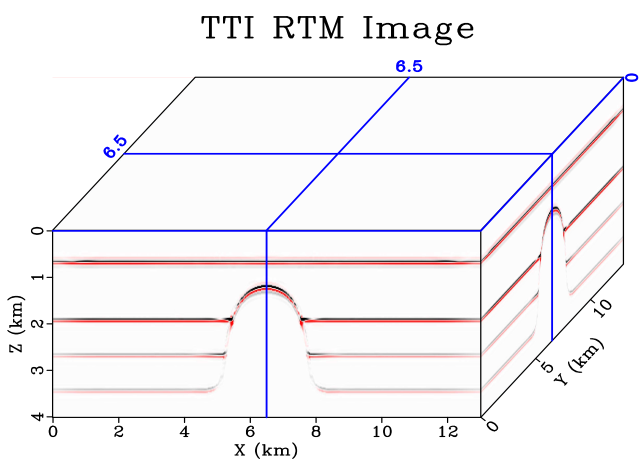

Figure 7: TTI RTM image of the 3D salt dome model.

Saudi Arabia for the computer cycles provided to this project. We also would like to thank BP for making the 2D TTI model and data set available. We acknowledge the anonymous reviewers for their valuable comments and suggestions.

References

Alkhalifah, T., 1998, Acoustic approximations for processing in transversely isotropic media: Geophysics, **63**, 623–631.

———, 2000, An acoustic wave equation for anisotropic media: Geophysics, **65**, 1239–1250.

Bos, L. and M. A. Slawinski, 2010, Elastodynamic equations: Characteristics, wavefronts and rays: The Quarterly Journal of Mechanics and Applied Mathematics, **63**, 23–38.

Chu, C., B. K. Macy, and P. D. Anno, 2011, Approximation of pure acoustic seismic wave propagation in tti media: Geophysics, **76**, WB97–WB107.

Crawley, S., S. Brandsberg-Dahl, J. McClean, and N. Chemingui, 2010, TTI reverse time migration using the pseudo-analytic method: The Leading Edge, **29**, 1378–1384.

Du, X., R. Fletcher, and P. J. Fowler, 2008, A new pseudo-acoustic wave equation for VTI media: 70th Annual Conference and Exhibition, EAGE, Extended Abstracts, H033.

Duveneck, E. and P. M. Bakker, 2011, Stable p-wave modeling for reverse-time migration in tilted ti media: Geophysics, **76**, S65–S75.

Epstein, M., D. Peter, and M. A. Slawinski, 2012, Combining ray-tracing techniques and finite-element modelling in deformable media: The Quarterly Journal of Mechanics and Applied Mathematics, **65**, 87–112.

Etgen, J. T. and S. Brandsberg-Dahl, 2009, The pseudo-analytical method: Application of pseudo-laplacians to acoustic and acoustic anisotropic wave propagation: SEG Technical Program Expanded Abstracts, **28**, 2552–2556.

Fletcher, R., X. Du, and P. J. Fowler, 2009, Reverse time migration in tilted transversely isotropic (TTI) media: Geophysics, **74**, WCA179–WCA187.

Fowler, P. J., X. Du, and R. P. Fletcher, 2010, Coupled equations for reverse time migration in transversely isotropic media: Geophysics, **75**, S11–S22.

Harlan, W., 1995, Flexible seismic traveltime tomography applied to diving waves: Stanford Exploration Project report, **89**, 145–164.

Kosloff, D. D. and E. Baysal, 1982, Forward modeling by a fourier method: Geophysics, **47**, 1402–1412.

Liu, F., S. A. Morton, S. Jiang, L. Ni, and J. P. Leveille, 2009, Decoupled wave equations for P and SV waves in an acoustic VTI media: SEG Technical Program Expanded Abstracts, **28**, 2844–2848.

Pestana, R. C., B. Ursin, and P. L. Stoffa, 2012, Rapid expansion and pseudo spectral implementation for reverse time migration in vti media: Journal of Geophysics and Engineering, **9**, 291.

Reshef, M., D. Kosloff, M. Edwards, and C. Hsiung, 1988, Threedimensional acoustic modeling by the fourier method: GEOPHYSICS, **53**, 1175–1183.

Thomsen, L., 1986, Weak elastic anisotropy: Geophysics, **51**, 1954–1966.

Zhan, G., R. C. Pestana, and P. L. Stoffa, 2012, Decoupled equations for reverse time migration in tilted transversely isotropic media: Geophysics, **77**, T37–T45.

Zhou, H., G. Zhang, and R. Bloor, 2006a, An anisotropic acoustic wave equation for VTI media: 68th Annual Conference and Exhibition, EAGE, Extended Abstracts, H033.

———, 2006b, An anisotropic acoustic wave equation for modeling and migration in 2D TTI media: SEG Technical Program Expanded Abstracts, **25**, 194–198.